Supporting information

S1 Data analysis of FIGAERO-CIMS

Data from the FIGAERO-CIMS was analysed with Tofware (Aerodyne Research, Inc. and Tofwerk AG) and Igor Pro (WaveMetrices Inc.). The initial mass calibration was conducted on I^-, IH_2O^-, $IHNO_3^-$, and I_3^-. In addition, the chemical composition of the 2−3 major dimer peaks were confirmed by the compounds measured simultaneously by the EESI-TOF, and these clearly identified ions were used as mass calibrants as well for the mass range higher than 400 Th. After processing the high resolution (HR) ion fits, the subsequent treatment of the processed HR data was performed using code written with MATLAB for checking signal to noise ratio, integrating thermogram data, etc.

S1.1 Background subtraction

For each experiment, one particle blank (zero sampling time + normal heating) was performed during dark aging. Because the background signal varies for each filters/experiment, when subtracting the background from the signals of normal filters, the integrated area of the particle blank from the same experiment was scaled up/down with a scaling factor. This factor was determined by comparing the detected signals of the last 1min of "temp soak" of the normal heating to the detected signals of the last 1min of "temp soak" of the zero heating) (Fig. S1).

S1.2 Impact of thermal decomposition on FIGAERO particle phase measurement

For the FIGAERO inlet, the artifacts associated with thermal decomposition were discussed in many previous studies (Lopez-Hilfiker et al., 2015; D'Ambro et al., 2019; Stark et al., 2017). We corrected the impact of thermal decomposition for further analysis on the chemical composition and temperature at maximum desorption rate (T_{max}) with the following steps:

(1) If the thermogram of a compound exhibited multiple peaks (Fig. S2a), T_{max} was determined based on the first peak, and the peak area was integrated only for the first peak.
(2) If the thermogram of a compound was monomodal, but T_{max} was "too high" based on its chemical composition (e.g., $C_5H_{10}N_2O_9$ has a similar T_{max} as that of $C_{10}H_{17}N_3O_{13}$, Fig. S2b), this compound was excluded from the analysis of the chemical composition.

S1.3 Uncertainties in the gas-phase measurement

The uncertainties in the gas-phase measurement due to the changing ratios of I^-/NO_3^- were tested after Exp. 2 (isoprene + NO_3). The total gas phase flow for the FIGAERO-CIMS was 5 L min^{-1} and it was

partly replaced by 1.5, 3.0, 4.0 L min^{-1} N_2 with keeping the total flow constant, causing I^-/NO_3^- = 0.09 (no dilution), 0.14, 0.28 and 1.6. In Fig. S3, three major gas-phase compounds $C_5H_{10}IN_2O_8^-$, $C_5H_9INO_6^-$, $C_5H_9IN_3O_{10}^-$ were chosen and their normalized signals (to the signals measured without dilution and with the consideration of dilution rates) were compared. The normalized signal didn't change significantly with decreasing I^-/NO_3^- as long as I^-/NO_3^- was higher than ~0.3, but it decreased about 20–40% when I^-/NO_3^- decreased further and was close to 0.1.

S2 Size dependence of light absorption

In Fig. S4, we simulated the difference between the mass absorption efficiency (m^2 g^{-1}, MAE) at wavelength = 350 nm of larger particles (diameter = 300 nm) versus smaller particles (diameter = 100 nm) as a function of an imaginary part of the refractive index using MiePlot, based on the equations found elsewhere (Bohren and Huffman, 1998). The imaginary part of the refractive index corresponds to species that absorb light. With a value of 0.001, the MAE of 300 nm particles is 1.7 times higher than the MAE of 100 nm particles. Although no direct measurement of the imaginary part of the refractive index was conducted in this study, based on a summary of different SOA systems by (Nakayama et al., 2015) and the study of He et al. (2021), a value between 0.001 and 0.01 could be expected for biogenic VOC species studied here.

SI Figures

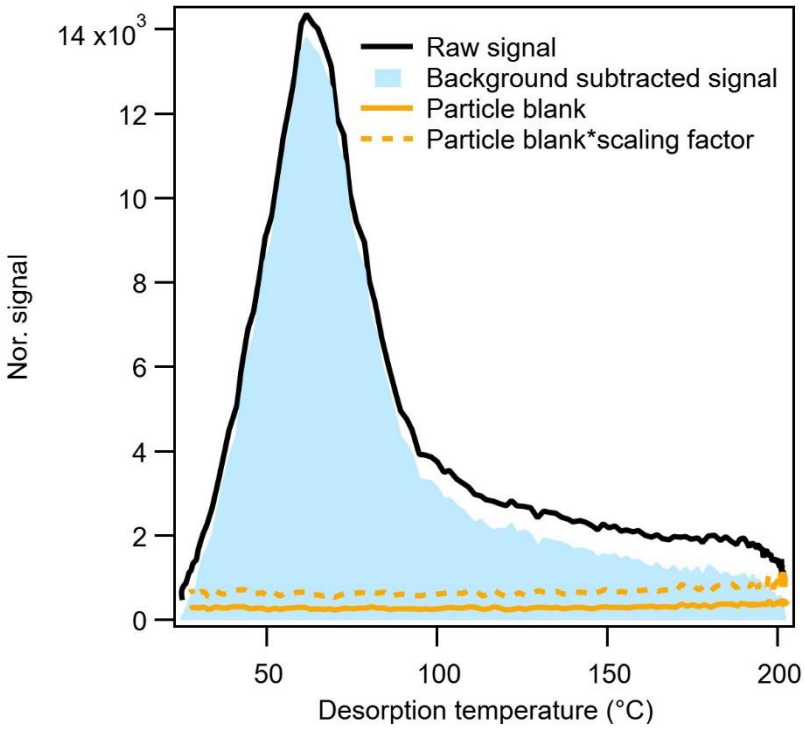

Fig. S1 Thermogram background subtraction for a typical compound $C_{10}H_{16}N_2O_{10}$ from Exp.2: isoprene + NO_3.

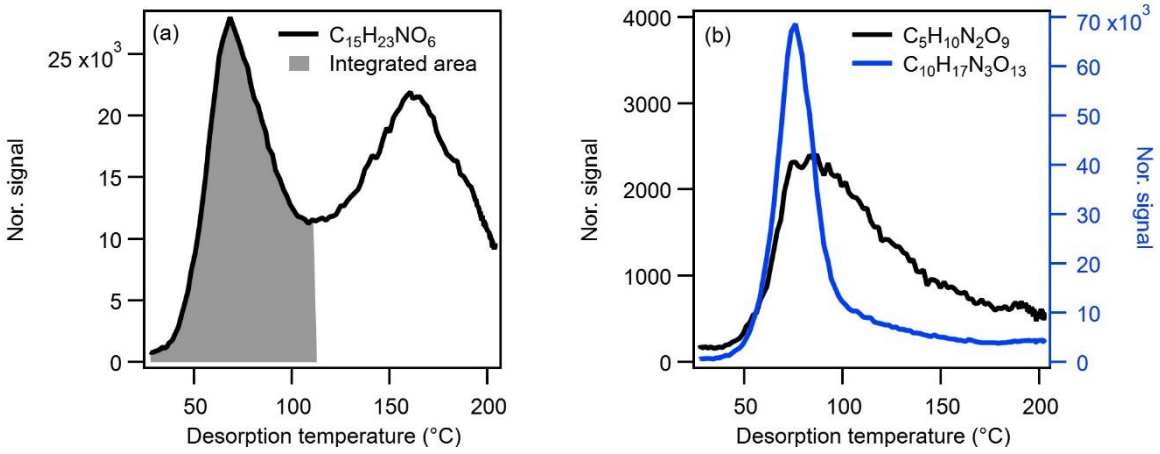

Fig. S2 (a) Thermogram of $C_{15}H_{23}NO_6$, the shaded area represents the integrated area. (b) Thermogram of $C_5H_{10}N_2O_9$, compared to that of $C_{10}H_{17}N_3O_{13}$ from a filter sample of Exp. 1: isoprene + NO_3.

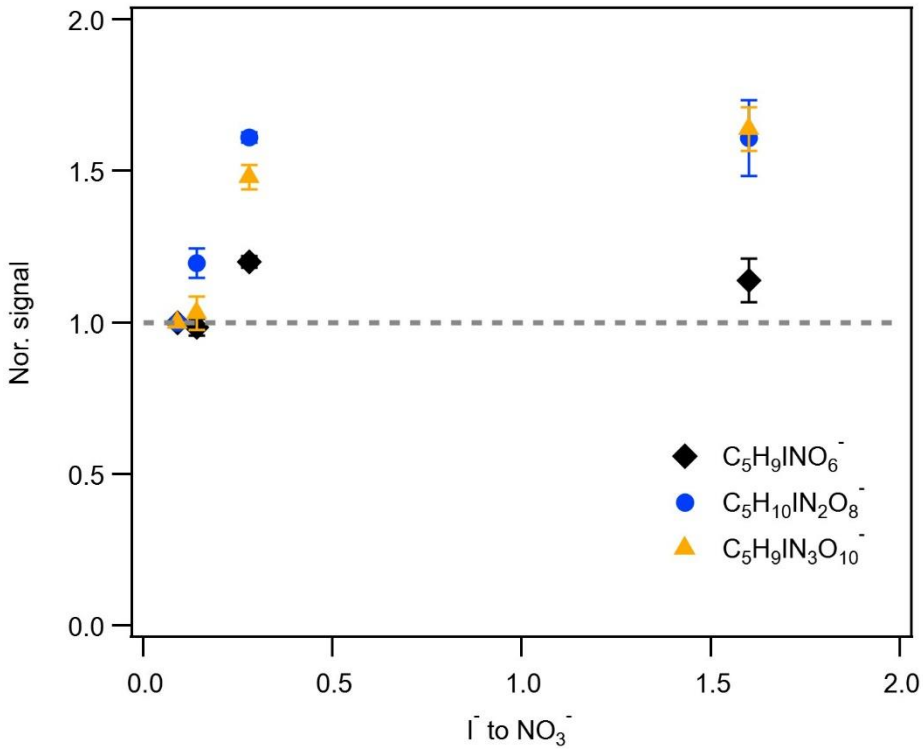

Fig. S3 Normalized signal of three major compounds in the gas phase from Exp. 2: isoprene + NO_3 as a function of I^-/NO_3^- ratio.

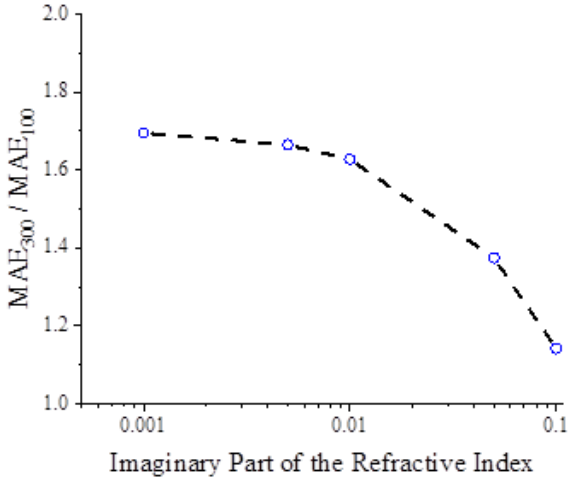

Fig. S4 Mass absorption efficiency (MAE) of 300 nm particles versus that of 100 nm particles at wavelength of 300 nm, as a function of imaginary part of the refractive index.

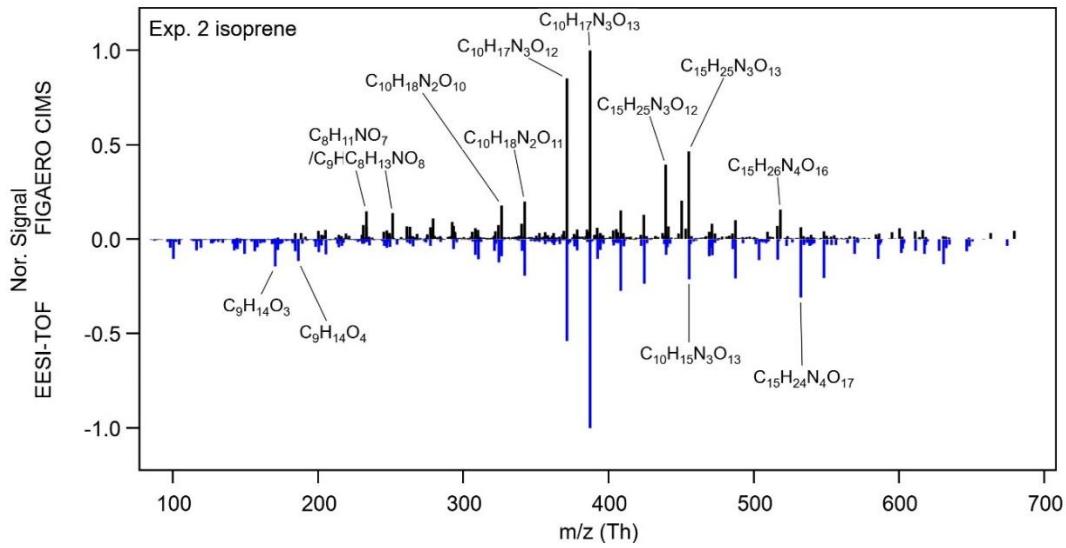

Fig. S5 FIGAERO-CIMS (positive axis) and EESI-TOF (negative axis) mass spectra of particle phase $C_xH_yO_zN_{0-4}$ formed during Exp. 2: isoprene + NO_3 shortly before photolysis. For the FIGAERO-CIMS, the last filter before photolysis is chosen. The EESI-TOF mass spectra are averaged mass spectra during the same sampling time as that of FIGAERO-CIMS. All mass spectra are normalized to the corresponding maximal signal.

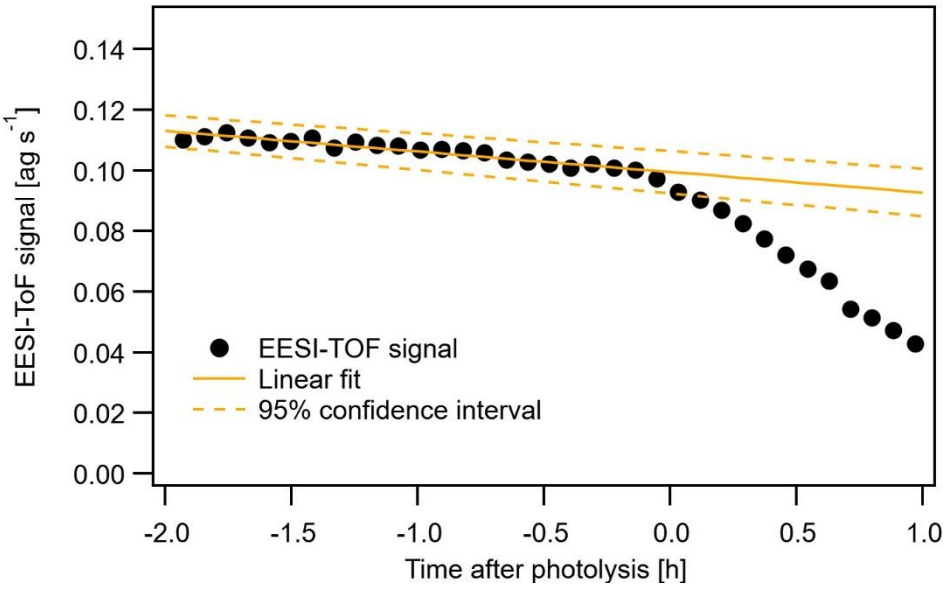

Fig. S6 Time series of $C_{10}H_{17}N_3O_{13}$ measured by the EESI-TOF and linear fit (with 95% confidence interval) of the 2 h pre-photolysis data points.

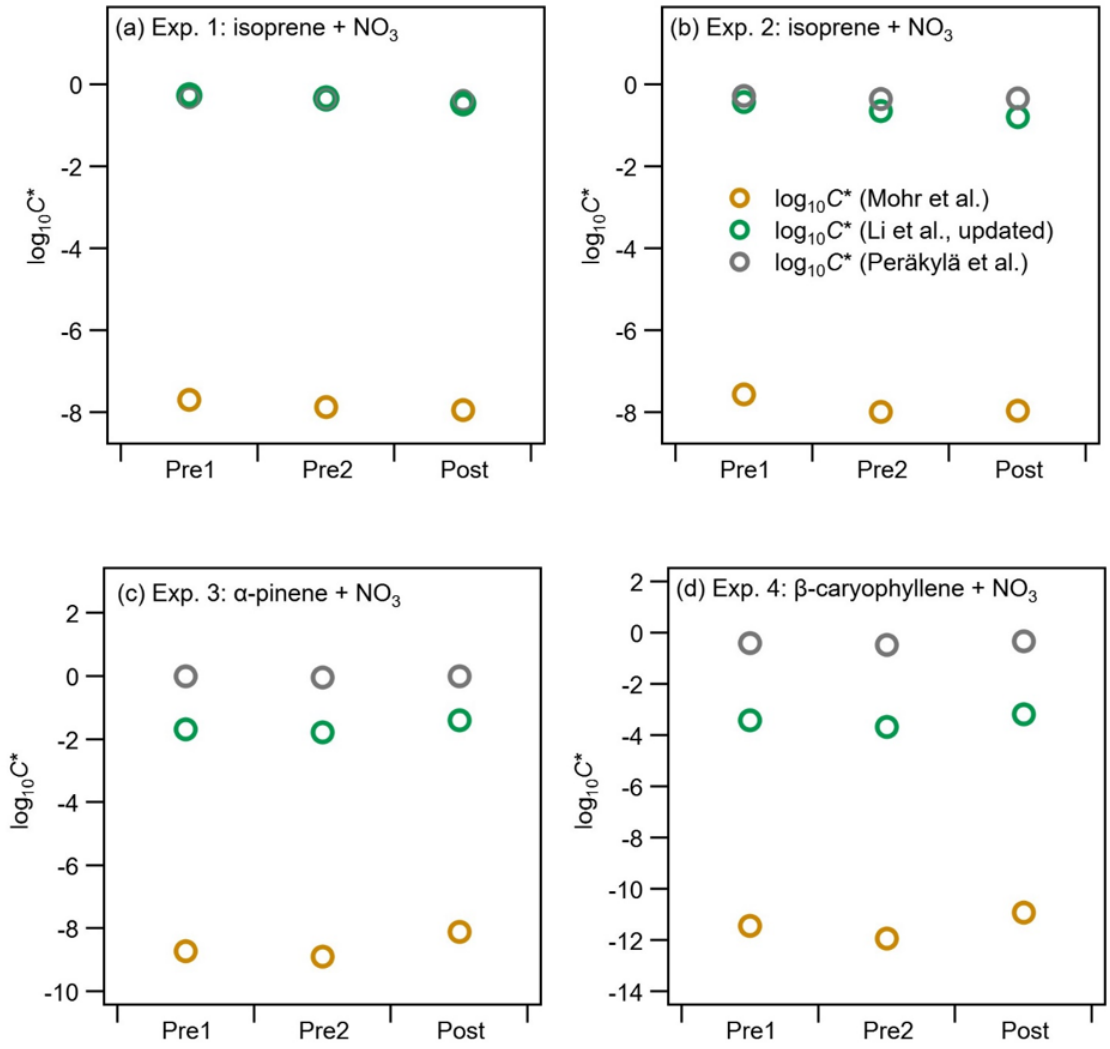

Fig. S7 Bulk $\log_{10}C^*$ calculated by Mohr et al. (2019), Li et al. (2016) (updated by Isaacman-VanWertz and Aumont (2020)), Peräkylä et al. (2020) for the three filters (Pre 1, Pre 2 and Post) from all experiments.

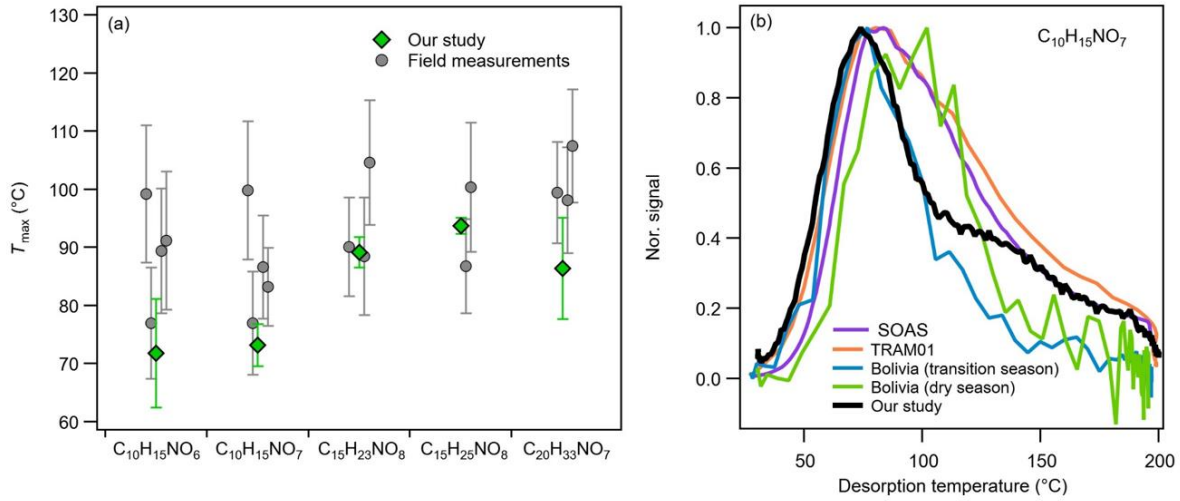

Fig. S8 (a) Comparison between the average T_{max} with standard deviation of $C_{10}H_{15}NO_{6,7}$, $C_{15}H_{23,25}NO_8$ and $C_{20}H_{33}NO_7$ from our study (mass loadings between ~0.3 and ~3 µg) including both dark aging and photolysis periods and three field campaigns: SOAS (Lopez-Hilfiker et al., 2016), TRAM01 (Huang et al., 2019) and the Bolivia campaign (during both transition season and dry season, Huang et al. in preparation). (b) Average thermograms of $C_{10}H_{15}NO_7$ from our study and the field campaigns. The mean mass loading was 0.33 ± 0.22, 1.45 ± 0.95, 0.07 ± 0.06 and 0.21 ± 0.16 µg, and the time of ramping the temperature of the nitrogen flow from ambient temperature up to 200 °C was 20, 15, 15 and 15 min for SOAS, TRAM01, Bolivia (transition season) and Bolivia (dry season), respectively.

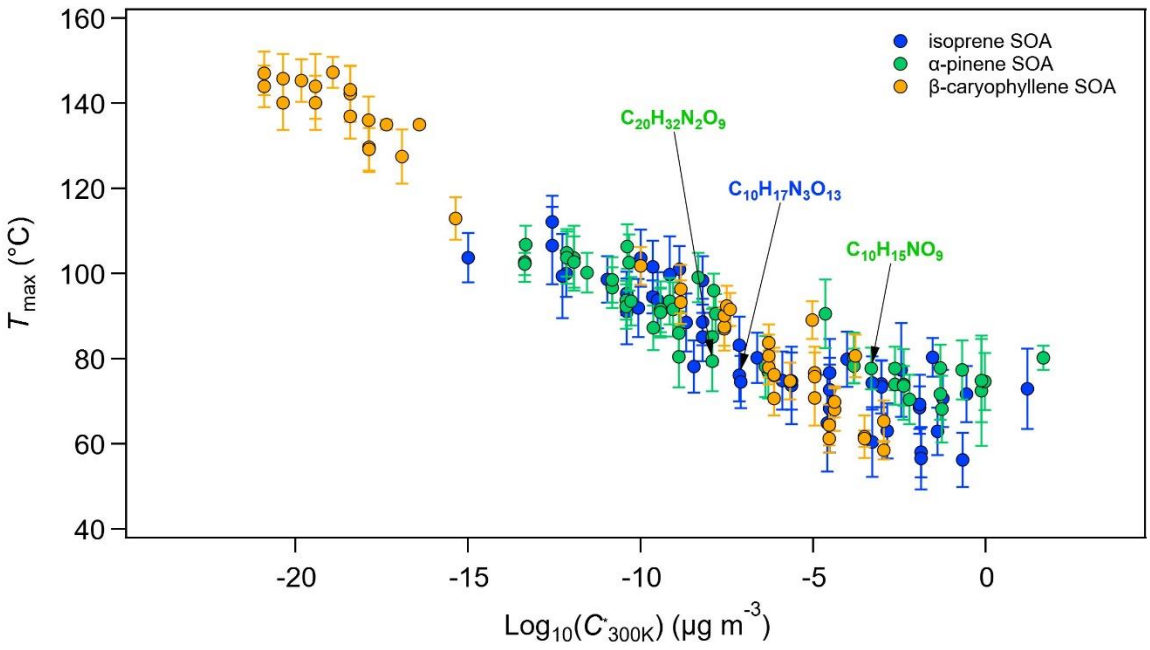

Fig. S9 Average T_{max} from all filter samples during dark aging and photolysis versus saturation concentration $\log_{10}C^*$ by Mohr et al. (2019) of top 50 compounds from the isoprene, α-pinene SOA and β-caryophyllene SOA.

SI References

Bohren, C. F., and Huffman, D. R.: Appendix a: Homogeneous sphere, Absorption and scattering of light by small particles, Wiley-VCH Verlag GmbH, 477482, 1998.

D'Ambro, E. L., Schobesberger, S., Gaston, C. J., Lopez-Hilfiker, F. D., Lee, B. H., Liu, J., Zelenyuk, A., Bell, D., Cappa, C. D., Helgestad, T., Li, Z., Guenther, A., Wang, J., Wise, M., Caylor, R., Surratt, J. D., Riedel, T., Hyttinen, N., Salo, V. T., Hasan, G., Kurtén, T., Shilling, J. E., and Thornton, J. A.: Chamber-based insights into the factors controlling epoxydiol (IEPOX) secondary organic aerosol (SOA) yield, composition, and volatility, Atmos. Chem. Phys., 19, 11253-11265, 10.5194/acp-19-11253-2019, 2019.

He, Q., Tomaz, S., Li, C., Zhu, M., Meidan, D., Riva, M., Laskin, A., Brown, S. S., George, C., Wang, X., and Rudich, Y.: Optical Properties of Secondary Organic Aerosol Produced by Nitrate Radical Oxidation of Biogenic Volatile Organic Compounds, Environmental Science & Technology, 55, 2878-2889, 10.1021/acs.est.0c06838, 2021.

Huang, W., Saathoff, H., Shen, X., Ramisetty, R., Leisner, T., and Mohr, C.: Chemical Characterization of Highly Functionalized Organonitrates Contributing to Night-Time Organic Aerosol Mass Loadings and Particle Growth, Environ Sci Technol, 53, 1165-1174, 10.1021/acs.est.8b05826, 2019.

Isaacman-VanWertz, G., and Aumont, B.: Impact of structure on the estimation of atmospherically relevant physicochemical parameters, Atmos. Chem. Phys. Discuss., 2020, 1-35, 10.5194/acp-2020-1038, 2020.

Li, Y., Pöschl, U., and Shiraiwa, M.: Molecular corridors and parameterizations of volatility in the chemical evolution of organic aerosols, Atmos. Chem. Phys., 16, 3327-3344, 10.5194/acp-16-3327-2016, 2016.

Lopez-Hilfiker, F. D., Mohr, C., Ehn, M., Rubach, F., Kleist, E., Wildt, J., Mentel, T. F., Carrasquillo, A. J., Daumit, K. E., Hunter, J. F., Kroll, J. H., Worsnop, D. R., and Thornton, J. A.: Phase partitioning and volatility of secondary organic aerosol components formed from α-pinene ozonolysis and OH oxidation: the importance of accretion products and other low volatility compounds, Atmos. Chem. Phys., 15, 7765-7776, 10.5194/acp-15-7765-2015, 2015.

Lopez-Hilfiker, F. D., Mohr, C., D'Ambro, E. L., Lutz, A., Riedel, T. P., Gaston, C. J., Iyer, S., Zhang, Z., Gold, A., Surratt, J. D., Lee, B. H., Kurten, T., Hu, W. W., Jimenez, J., Hallquist, M., and Thornton, J. A.: Molecular Composition and Volatility of Organic Aerosol in the Southeastern U.S.: Implications for IEPOX Derived SOA, Environmental Science & Technology, 50, 2200-2209, 10.1021/acs.est.5b04769, 2016.

Mohr, C., Thornton, J. A., Heitto, A., Lopez-Hilfiker, F. D., Lutz, A., Riipinen, I., Hong, J., Donahue, N. M., Hallquist, M., Petäjä, T., Kulmala, M., and Yli-Juuti, T.: Molecular identification of organic vapors driving atmospheric nanoparticle growth, Nature Communications, 10, 4442, 10.1038/s41467-019-12473-2, 2019.

Nakayama, T., Sato, K., Tsuge, M., Imamura, T., and Matsumi, Y.: Complex refractive index of secondary organic aerosol generated from isoprene/NO_x photooxidation in the presence and absence of SO_2, Journal of Geophysical Research: Atmospheres, 120, 7777-7787, https://doi.org/10.1002/2015JD023522, 2015.

Peräkylä, O., Riva, M., Heikkinen, L., Quéléver, L., Roldin, P., and Ehn, M.: Experimental investigation into the volatilities of highly oxygenated organic molecules (HOMs), Atmos. Chem. Phys., 20, 649-669, 10.5194/acp-20-649-2020, 2020.

Stark, H., Yatavelli, R. L. N., Thompson, S. L., Kang, H., Krechmer, J. E., Kimmel, J. R., Palm, B. B., Hu, W., Hayes, P. L., Day, D. A., Campuzano-Jost, P., Canagaratna, M. R., Jayne, J. T., Worsnop, D. R., and Jimenez, J. L.: Impact of Thermal Decomposition on Thermal Desorption Instruments: Advantage of Thermogram Analysis for Quantifying Volatility Distributions of Organic Species, Environmental Science & Technology, 51, 8491-8500, 10.1021/acs.est.7b00160, 2017.